NeuroImage 44 (2009) 35–42

Contents lists available at ScienceDirect

NeuroImage

journal homepage: www.elsevier.com/locate/ynimg

Detection of inter-hemispheric metabolic asymmetries in FDG-PET images using prior anatomical information

L. Zhou [a,b], P. Dupont [b,c,*], K. Baete [a], W. Van Paesschen [d], K. Van Laere [a], J. Nuyts [a,b]

[a] Nuclear Medicine, KU Leuven and UZ Leuven, Leuven, Belgium
[b] Medical Imaging Center, KU Leuven and UZ Leuven, Leuven, Belgium
[c] Cognitive Neurology, KU Leuven and UZ Leuven, Leuven, Belgium
[d] Experimental Neurology, KU Leuven and UZ Leuven, Leuven, Belgium

ARTICLE INFO

Article history:
Received 24 June 2008
Revised 17 July 2008
Accepted 20 July 2008
Available online 3 August 2008

Keywords:
Asymmetry index
Positron emission tomography

ABSTRACT

[^{18}F] FDG positron emission tomography (PET) is commonly used to highlight brain regions with abnormal metabolism. Correct interpretation of FDG images is important for investigation of diseases. When the FDG uptake is compared between hemispheres, confusion can arise because it might be difficult to determine whether an observed asymmetry is physiological and due to normal anatomical variation or pathological. In this paper we propose a new method, which calculates an anatomy-corrected asymmetry index (ACAI), to highlight inter-hemispheric metabolic asymmetry in FDG images without the influence of anatomical asymmetry. Using prior anatomical information from MRI, the ACAI method only takes into account voxels that belong to a certain anatomical class. For the evaluation of detection performance, this method is applied on homogeneous brain phantoms and realistic analytical simulated FDG-PET images with known asymmetries. Results from these simulations demonstrated the validity of ACAI and its potential perspective in the future.

Introduction

[^{18}F]fluorodeoxyglucose ([^{18}F]FDG) positron emission tomography (PET) is useful in the evaluation of neurological diseases, such as epilepsy, by detecting abnormalities in the cerebral glucose metabolism. In a number of pathologies usually one hemisphere is predominately affected. Comparing the metabolism in homologous regions between both hemispheres is a sensitive way of detecting hypo- or hypermetabolic regions. Therefore, the inter-hemispheric metabolic asymmetry is one of the most helpful information for the analysis of the FDG-PET image. Visual assessment of FDG-PET images is widely used in a clinical situation, but the results are observer-dependent. Therefore, quantification methods are needed for accurate diagnosis. Several methods have been proposed for detecting the functional asymmetry of the brain: a region of interest (ROI)-based or a volume of interest (VOI)-based method (Kang et al., 2001), voxel neighborhood-based methods (Aubert-Broche et al., 2003, 2005), voxel-based methods (Signorini et al., 1999; Van Bogaert et al., 2000) and methods based on global information (Volkau et al., 2006). However, these methods suffer from either the subjectivity of manually drawing the regions of interest, or the influence from the asymmetric anatomical structure of the human brain.

In this paper, we propose an unsupervised method to detect the inter-hemispheric metabolic asymmetry by calculating an anatomy-corrected asymmetry index (ACAI) of the investigated image. In comparison with the methods mentioned above, ACAI can effectively avoid the impact from the asymmetric structure of the brain, and only focus on the asymmetry caused by abnormal metabolism. The basic idea of ACAI method is to take advantage of the anatomical information obtained from magnetic resonance imaging (MRI), and construct an asymmetry indices (AI) map based on the classification of voxels. The algorithm of ACAI is concisely described and a validation procedure is performed by a set of simulation images to evaluate the detection performance of this new method.

Materials and methods

Firstly, we describe the definition of a conventional AI (Aubert-Broche et al., 2005), which is referred as non-corrected asymmetry index (NCAI) in contrast to ACAI. Then the basic algorithm of ACAI as well as its implementation process in the practical application is explained in detail. Lastly, the simulation experiments which were used to validate our ACAI method are described.

Definition and algorithm

NCAI

Assume that for a target image, whose inter-hemispheric asymmetries need to be investigated, the mid-sagittal plane is well defined.

* Corresponding author. Labo for Cognitive Neurology and Medical Imaging Center, O&N II, Herestraat 49, bus 1022, 3000 Leuven, Belgium.
E-mail address: patrick.dupont@med.kuleuven.be (P. Dupont).

1053-8119/$ – see front matter © 2008 Elsevier Inc. All rights reserved.
doi:10.1016/j.neuroimage.2008.07.047

Taking a volume of interest (VOI) and its homologous VOI in this target image, the mean intensity of the voxel values within each VOI can be estimated. NCAI is thus calculated by comparing these two mean intensity values. The whole procedure can be considered as two steps: step 1 is a convolution between the target image and a certain convolution kernel (weighting), which generates a volumetric image VI_{NC}. Step 2 is the subtraction between VI_{NC} and its homologous image (which is the same image but flipped around the mid-sagittal plane), generating the NCAI map. The basic idea of NCAI can be depicted as the following equations:

$$VI_{NC}(i) = \frac{\sum_{j\in K_i} w_{ij}T_j}{\sum_{j\in K_i} w_{ij}} \quad (1)$$

$$NCAI(i) = 200 \times \frac{VI_{NC}(i) - VI_{NC}(i')}{VI_{NC}(i) + VI_{NC}(i')} \quad (2)$$

where $VI_{NC}(i)$ is the value of the volumetric image in voxel i, K_i is the convolution kernel centered in voxel i, w_{ij} is the weight of K_i at voxel j, T_i is the value of the target image in voxel i, i' is the homologous voxel of i. Note that in the calculation of NCAI, all voxels in the target image are taken into account at the convolution and subtraction steps.

ACAI

Assume that the target image (e.g. the FDG image) and its MRI-based fuzzy segmentations are available with high image quality, and already well coregistered. Normally the segmentation images are the fraction images of N different tissue classes (e.g. gray matter (GM), white matter (WM), cerebrospinal fluid (CSF), etc.). The values of the voxels in the segmentation images are between 0 and 1, representing the probability that the voxel belongs to that specific tissue class. Depending on the application, segmentation images of tissue classes of interest are selected, leading to the anatomical information that will be used. In this article we aimed at investigating the metabolic abnormalities in the FDG image in the gray matter of patients with partial epilepsy. Therefore the segmentation of gray matter was selected as the prior anatomical information used for further calculation.

Similar to NCAI, there are also a convolution step and a subtraction step in the ACAI calculation. Only voxels that belong to the tissue of interest, i.e. the voxels that have a non-zero probability in the segmentation map, are considered into the convolution step. In our study, only voxels having a non-zero GM probability are taken into consideration. This is done by limiting the weighting of the convolution kernel to these voxels and by weighting the voxels according to the convolution kernel and the probabilities given by the segmentation map. The weighted sum is normalized by the total weight of the GM voxels covered by that kernel. This step results in a volumetric image VI_{AC}. The whole basic idea can be concisely written as Eq. (3):

$$VI_{AC}(i) = \frac{\sum_{j\in K_i\cap A} w_{ij}a_jT_j}{\sum_{j\in K_i\cap A} w_{ij}a_j} \quad (3)$$

where $VI_{AC}(i)$ is the value of the volumetric image in voxel i, A is the segmentation map for the tissue class of interest, and a_j is the probability of the segmentation (i.e. the value of A) in voxel j used as the prior anatomical information. In principle, any kernel with a symmetrical shape can be used in this procedure. This algorithm can be used for calculating the volumetric images of different tissue classes simultaneously. However, in this article we only use the segmentation A of the GM.

To acquire the ACAI map of a certain tissue class defined by the segmentation A, again every voxel in the volumetric image is compared with its homologous voxel. The ACAI are thus defined as:

$$ACAI(i) = \begin{cases} 200 \times \frac{VI_{AC}(i) - VI_{AC}(i')}{VI_{AC}(i) + VI_{AC}(i')} & i\in A \\ 0 & i\notin A \end{cases} \quad (4)$$

Note that only voxels localized in that segmentation map A is maintained in the final ACAI map, all the rest are set to zero.

Validation

In order to evaluate the performance of our new method, we used different phantoms (see below). Comparison was made between ACAI and NCAI methods. Mean values of AI within a certain region of interest acquired from both methods were calculated and compared with referential asymmetry indices.

To validate the ability of our ACAI method in eliminating the anatomical asymmetries, a 3-D digital software phantom, which is provided by the BrainWeb database at McGill University (Montreal, Canada, http://www.bic.mni.mcgill.ca/brainweb/), was used as a perfect image in our experiment. The dimensions of the software phantom are 181×217×181 voxels with an isotropic voxel size of 1 mm. GM, WM and CSF were identified by the discrete anatomical model, in which each voxel was classified into a certain tissue class. This software phantom can be considered as an ideal brain phantom since the signal in every tissue class is homogeneous, and every voxel is clearly classified into either GM, WM or CSF. For the simulation of metabolic abnormalities, four 3-D regions within GM were delineated (Baete et al., 2004b) on this brain phantom as region of interest (ROI) by MRIcro software (http://www.mricro.com/). The locations and the sizes of these four ROIs are given in Fig. 1. The signal was increased by 20% in these regions. From here onwards, we call the brain phantom without the additional hyperintense ROI "baseline phantom", while the brain phantom with those ROI is called "asymmetric phantom".

For the validation of our method on realistic images, a set of simulated FDG images were constructed based on these two digital brain phantoms. Accordingly, baseline and asymmetric FDG images were generated during the simulation, which represented the normal

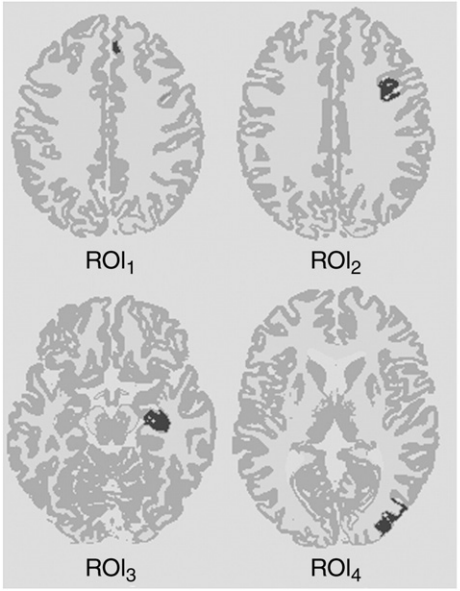

ROI	Size (cm³)
1	0.14
2	0.96
3	1.73
4	2.41

Fig. 1. Locations and the size of four hypermetabolic 3-D ROIs that were used in the simulation experiments. The location of each ROI is visualized in black for the central plane through the ROI.

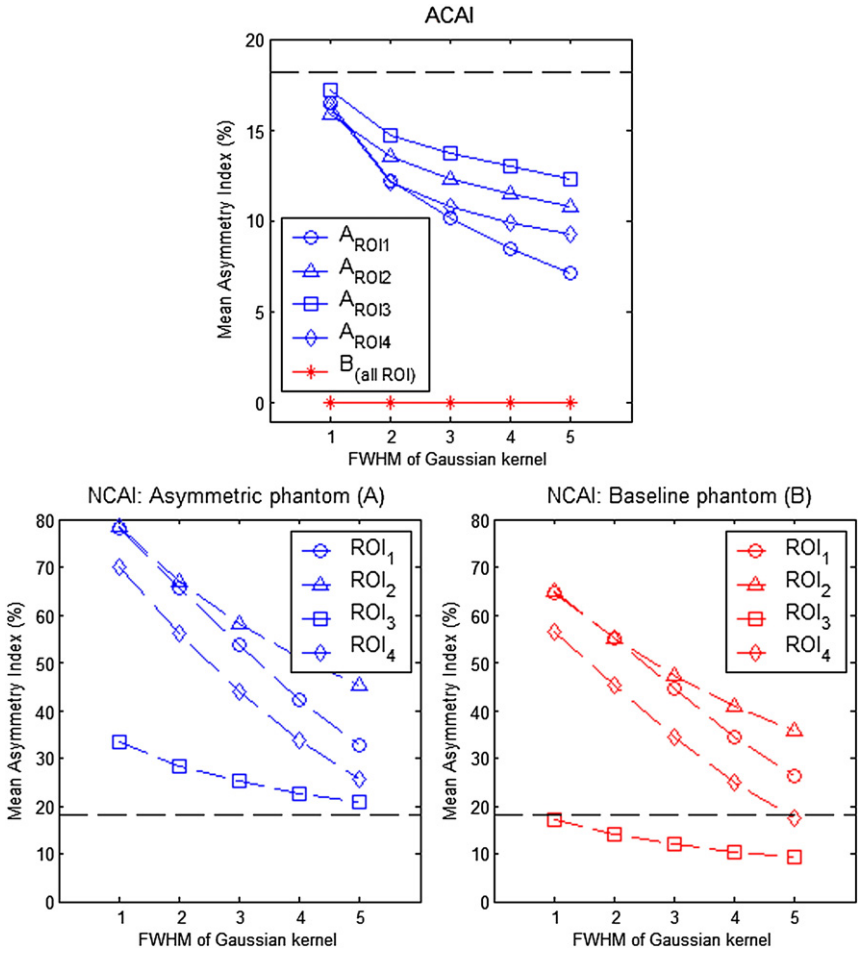

Fig. 2. Mean AI (both ACAI and NCAI) of each ROI in the original brain phantoms (dimensions 181×217×181) calculated using a Gaussian kernel. A and B are short for "Asymmetric" and "Baseline" phantom, respectively. The dashed line represents the true AI value. Note that ACAI of all ROI in the baseline image are almost zero.

FDG-PET of a human brain and the one with additional metabolic abnormalities, respectively. To simulate the tracer distribution in normal human brain, tracer activity uptake was set to 4 counts/mm^3 in GM, 1 count/mm^3 in WM, and no uptake in CSF. In the simulated asymmetric phantoms, the tracer activity uptake in the four regions of interest was increased by 20%. Sinograms of a simulated PET were generated from the brain phantoms as described by Baete et al. (2004a,b). With the tracer uptake values measured above, a realistic number of counts in the sinograms was obtained. Poisson noise was added to these sinograms and the reconstruction was performed including the attenuation correction and using ordered subset expectation maximization (OSEM) (Hudson and Larkin, 1994) using the following iteration scheme (iteration×subset): 1×18, 1×16, 1×12, 1×8, 1×6, 1×3. For each tracer uptake image, 100 different Poisson noise realizations were derived, generating 100 different pairs of images. The dimensions of the simulated FDG images are 100×100×73 voxels, with an isotropic voxel size of 2.25 mm.

Two referential AI values were adopted in our study. One is the true AI which is in accord with the 20% added hyperintensity in ROIs:

$$\mathrm{AI}_{\mathrm{true}} = 200 \times \frac{1.2-1}{1.2+1} = 18.18\%$$

The other is the "best" AI that we can obtain in each ROI given the simulated PET scanner. Due to the limited spatial resolution of PET scanner, the referential AI values $\mathrm{AI}^{\mathrm{ref}}_{\mathrm{ROI}}$ are much lower than $\mathrm{AI}_{\mathrm{true}}$. To acquire $\mathrm{AI}^{\mathrm{ref}}_{\mathrm{ROI}}$, mean images of 100 baseline and 100 asymmetric FDG phantoms were computed and subtracted. The referential AI in each ROI is defined by

$$\mathrm{AI}^{\mathrm{ref}}_{\mathrm{ROI}} = 200 \times \frac{\overline{A}_{\mathrm{ROI}} - \overline{B}_{\mathrm{ROI}}}{\overline{A}_{\mathrm{ROI}} + \overline{B}_{\mathrm{ROI}}} \tag{5}$$

where $\overline{A}_{\mathrm{ROI}}$ and $\overline{B}_{\mathrm{ROI}}$ represent the mean value of a certain ROI in the mean asymmetric image and the mean baseline image, respectively.

For the evaluation, first, both methods (NCAI and ACAI) were applied on the original digital brain phantoms, in order to estimate their ability in dealing with two different asymmetries (anatomical and metabolic) in such perfect images. Then, both methods were applied to the 100 baseline and 100 asymmetric simulated images to estimate their performance on the realistic FDG images. A Gaussian kernel was adopted in all simulations, with its full width at half maximum (FWHM) ranging from 1 to 5 voxels. On the resultant asymmetry index maps, mean AI of all voxels within each ROI was calculated. Results from the two methods were compared for each ROI. The true AI and the referential AI obtained from the mean images were used to evaluate to what extent the metabolic asymmetries can be detected and the anatomical asymmetries can be minimized by the method with prior anatomical information.

Implementation

The algorithm was implemented as follows: the first step was to rigidly coregister the MRI and the MRI-based segmentation images to the target image (or vice versa). Segmentation and registration were

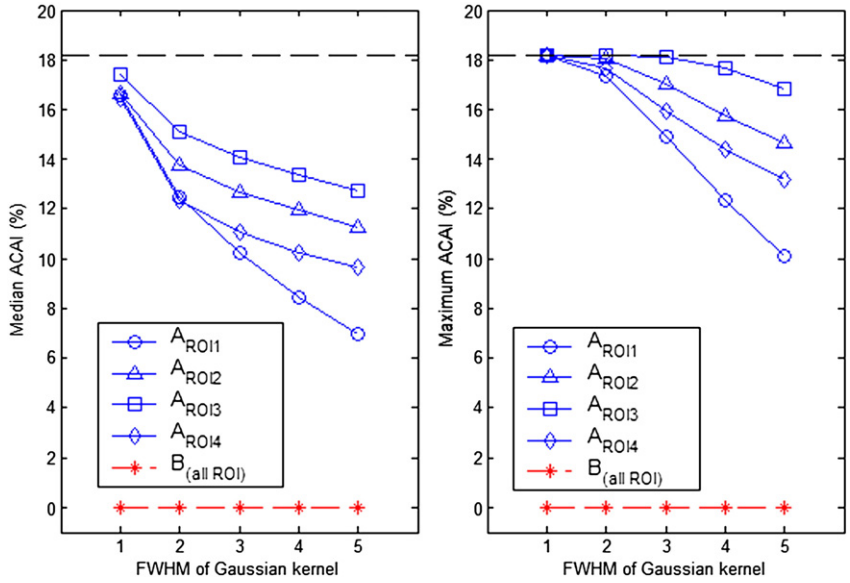

Fig. 3. Median and maximum ACAI of each ROI of the original brain phantom with 4 induced hypermetabolic regions calculated using a Gaussian kernel. A and B are short for "Asymmetric" and "Baseline" phantom, respectively. The dashed line represents the true AI value.

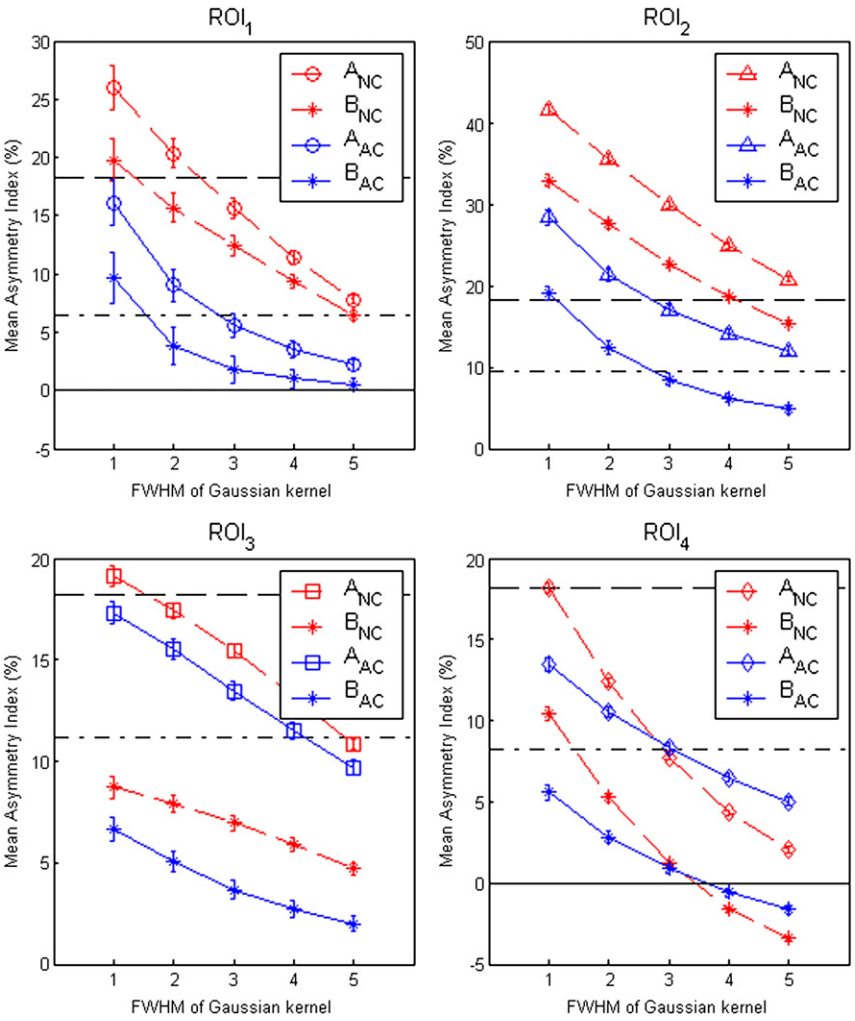

Fig. 4. Mean AI of 100 baseline and 100 phantom images acquired by both methods using a Gaussian kernel. The standard deviations of AI values across 100 images are plotted as well. A and B are short for "Asymmetric" and "Baseline" FDG images, respectively. ACAI curves are plotted by solid lines, while NCAI curves are depicted by dashed lines. The two horizontal lines represent the true AI value (dashed line) and the referential AI in each ROI (dash-dotted line), respectively.

performed using SPM2 (http://www.fil.ion.ucl.ac.uk/spm/). In order to define the mid-sagittal plane in an automatic way, all these images were warped to the Montreal Neurological Institute (MNI) space using the PET template provided in SPM2. The prior anatomical information was extracted from the segmentation images of a certain tissue class. The volumetric images (VI_{NC}, VI_{AC}) were computed according to Eq. (1) and Eq. (3). To determine the homologous regions on the two hemispheres automatically, both volumetric images were flipped along the mid-sagittal plane. Voxels located at the corresponding place in the original and the flipped volumetric images were considered as a pair of homologous voxels. The outcome NCAI and ACAI maps were then calculated by Eq. (2) and Eq. (4), respectively. Both methods were implemented in MATLAB 6.5, Release 13.

Application

To demonstrate that the ACAI method can be applied on real data, a FDG image of an epilepsy patient showing visually a metabolic asymmetry and the corresponding MRI image was selected. The FDG image and the anatomical MRI (3-D MPRAGE) were acquired according to the standard clinical protocol. Segmentation and warping into MNI space was done using SPM2.

Results

Fig. 2 depicts AI values (both ACAI and NCAI) of the original brain phantoms (dimensions 181×217×181) using a Gaussian kernel. For each ROI, the mean ACAI and the mean NCAI (shortly referred as "ACAI" and "NCAI" in the following text) over the whole region were calculated. As theoretically predicted, for the baseline brain phantom, ACAI in every ROI almost equals zero. For the asymmetric brain phantom, ACAI clearly depicts the inter-hemispheric functional asymmetries in 4 induced hyperintense regions. Using a FWHM of 1 voxel for the Gaussian kernel, ACAI in these ROIs are very close to AI_{true}. The underestimation of the true value is due to voxels at the border of each region which have a lower AI, therefore we also show the median and the maximum ACAI values (Fig. 3). As expected, the maximum ACAI values are higher and much closer to the true AI value. In the remainder of the text, we will only report the results on the mean AI values.

The NCAI curves of the original brain phantoms are shown in the lower row in Fig. 2. With NCAI, large asymmetries are detected in the baseline brain phantom which has no intensity variation but only the anatomical asymmetries. NCAI of the baseline phantom varies greatly from ROI to ROI and depends on the kernel size. For the asymmetric phantom, an increase of NCAI is detected at each ROI compared to the baseline case. Obviously, NCAI contains both the anatomical and functional asymmetries, which cannot be separated by this method.

The results reported in Figs. 2 and 3 are for the high-resolution phantoms in an ideal situation. However, when a PET measurement is simulated, the results will include the effect of the limited spatial resolution of the scanner and of noise introduced during the measurement. The results in that case are shown in Fig. 4. The ACAI and NCAI curves of 100 baseline and 100 asymmetric simulated FDG images, calculated with the Gaussian kernel, are plotted as function of the FWHM of the Gaussian kernel for the different regions of interest. Each point on the curve represents the mean AI of 100 simulation images in a certain ROI calculated at a certain kernel size. The results of NCAI are similar with those obtained from the original brain phantoms. In comparison with NCAI, ACAI method remarkably reduces the residual AI in the baseline images. In most ROIs, the ACAI of the baseline are much closer to zero, which means that the asymmetries due to anatomical variation are greatly minimized. Furthermore, the difference in asymmetry (between the asymmetric phantom and the baseline phantom) is always larger for ACAI compared to NCAI.

Fig. 5 shows an example of a reconstruction of one single noise realization in a transaxial slice through ROI 2 (both for the asymmetric and the baseline phantom) using a Gaussian kernel with 5 voxels FWHM. NCAI shows a clear asymmetry near ROI 2 in the asymmetric image, but this is also the case for the baseline phantom. Furthermore, several other regions (with no metabolic asymmetry in the original phantom) also show obvious asymmetries. The ACAI method shows little asymmetry in the baseline phantom and a clear – but smaller –

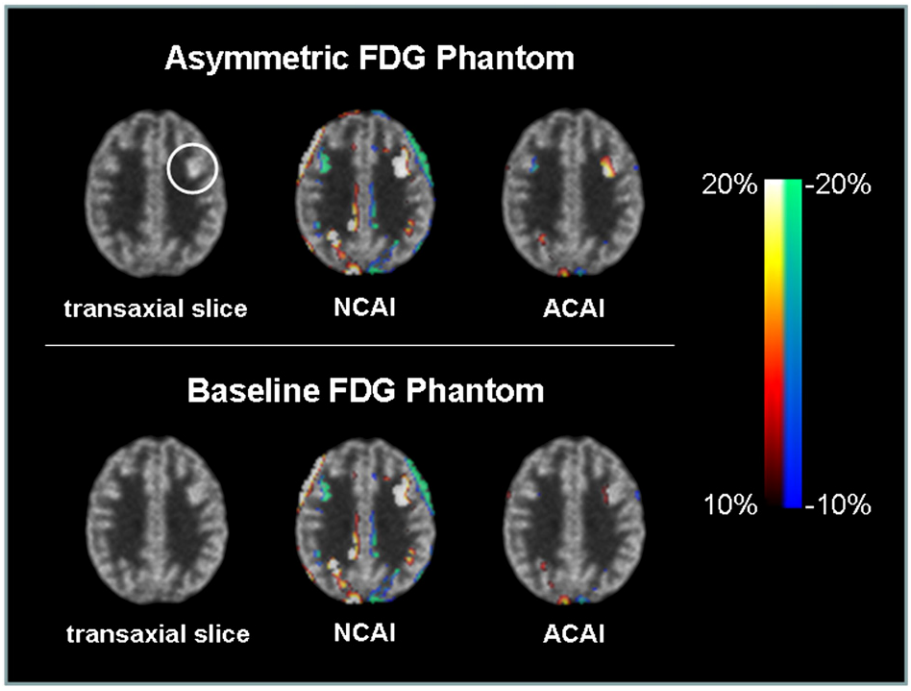

Fig. 5. An example of the method applied on a single noise realization using a Gaussian kernel with a FWHM of 5 voxels. Top row gives the reconstruction of an axial slice through ROI 2 (marked by the white circle) for the asymmetric image, as well as the corresponding NCAI/ACAI overlay image. The bottom row shows the same for the baseline image.

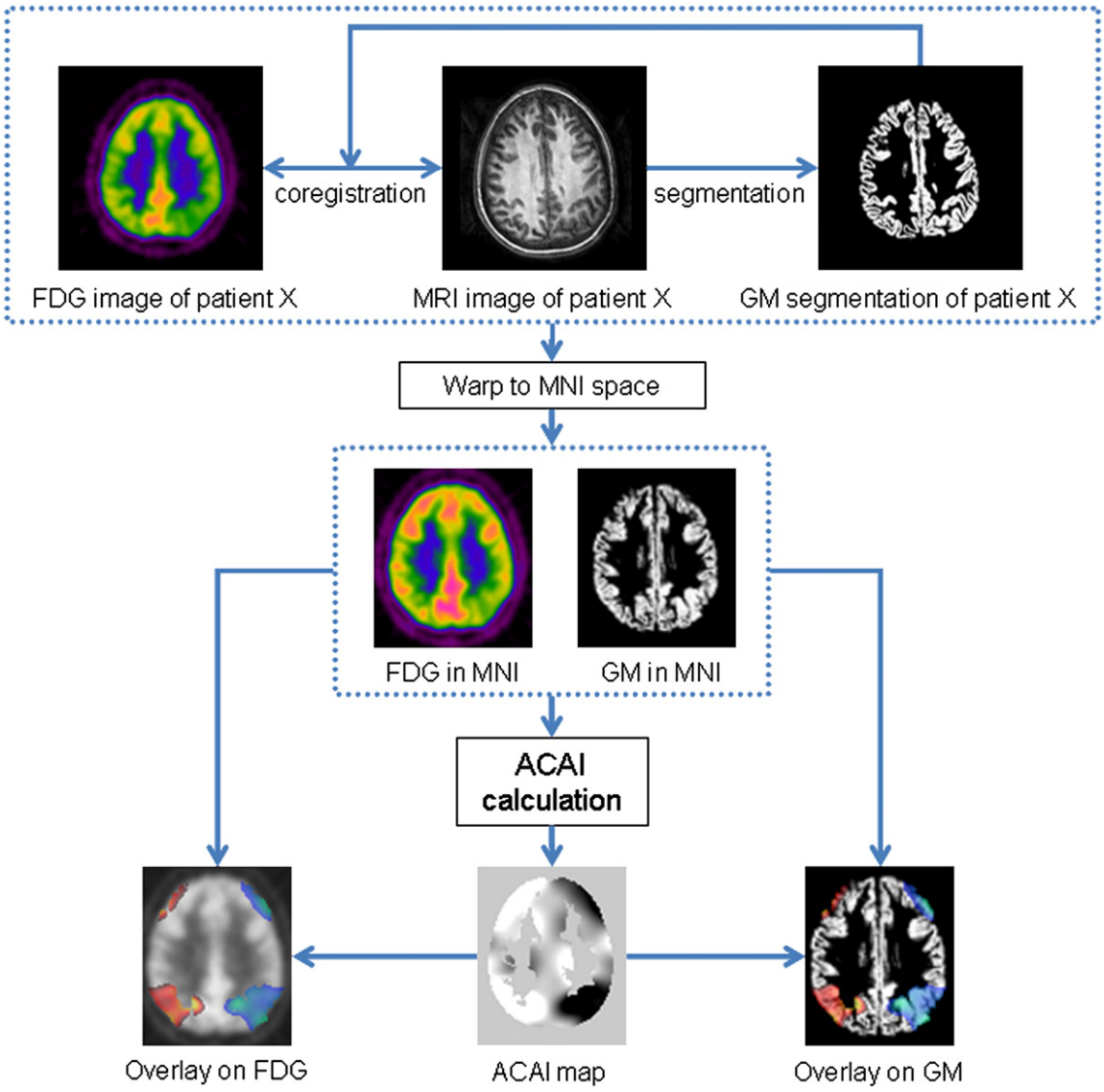

Fig. 6. A schematic figure of the application of the ACAI method in a clinical environment.

asymmetry in ROI 2 and almost no other voxels with an asymmetry of 10% or more in the asymmetric phantom.

Fig. 6 depicts a schematic figure of the application of the ACAI method in a clinical environment. An example of this method on real patient data is shown in Fig. 7. Segmentations were obtained using SPM2. For the real patient data we applied a Gaussian kernel with 9 voxels FWHM. This clearly depicts the area of asymmetric metabolism. For the NCAI method, a large kernel is a disadvantage because different tissue classes are intermixed. Therefore, we also show the results of NCAI when using a smaller Gaussian kernel (FWHM=3 voxels).

Discussion

The proposed ACAI method aims at detecting inter-hemispheric metabolic asymmetries in brain FDG-PET images without the influence of anatomical asymmetries due to the intrinsic local asymmetrical structure of human brain. For this purpose, prior anatomical information obtained from MRI segmentation is integrated into the voxel-based computation to calculate the inter-hemispheric difference. In comparison with the conventional NCAI method, our method can highlight the metabolic asymmetries in the outcome AI map by taking into account the anatomical asymmetries. Useful information about the abnormal metabolism can be picked up more easily and clearly by the proposed method.

Factors that affect the results

Our simulated baseline images only have anatomical asymmetries, while the simulated phantom images contain both anatomical and metabolic asymmetries. The challenge is to solely pick out inter-hemispheric metabolic differences in simulated images, while removing all influences from anatomical asymmetries. The experiment on the original homogeneous brain image shows that the ACAI method achieves this in ideal, high-resolution images. Nevertheless, when data are used which simulate the reconstruction of a PET measurement (including statistical noise and limited spatial resolution) ACAI was only partially successful in removing the anatomical asymmetries: e.g. in ROI 2, where the residual AI is relatively large and cannot be neglected in the interpretation (Fig. 4).

There are several factors that can influence the outcome asymmetry indices map: the accuracy of MRI segmentation, the coregistration between MRI and FDG images, the accuracy of defining the homologous regions, the complexity of the ROI in combination

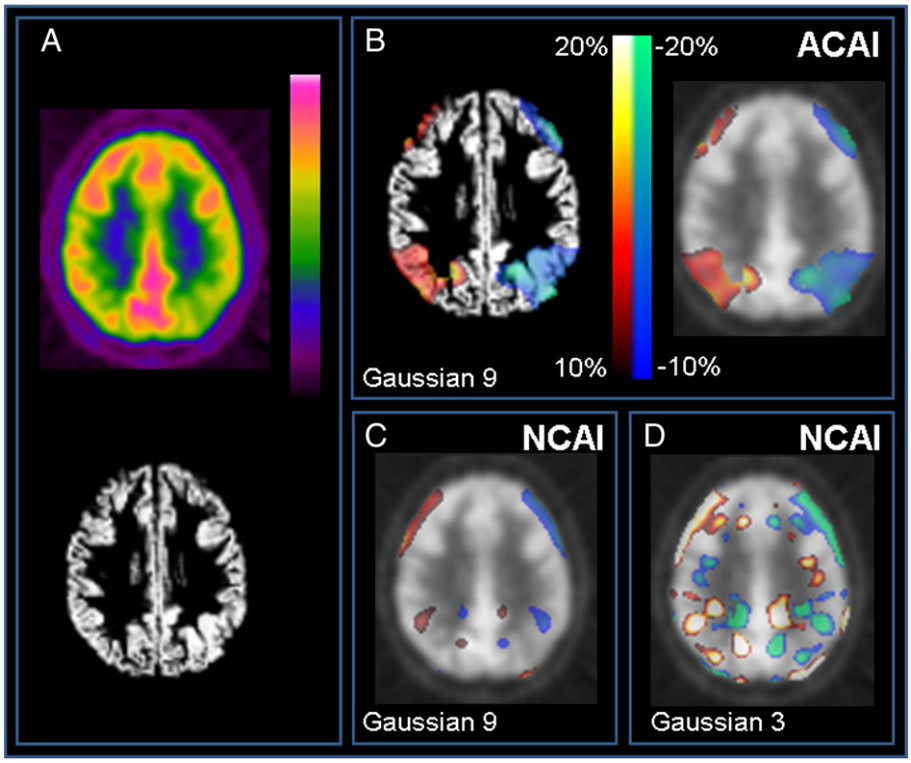

Fig. 7. The application of our ACAI algorithm on a FDG image of an epileptic patient. A transaxial slice of the original FDG image is shown (A) together with the GM segmentation map. The asymmetry index image overlayed on the GM or FDG images for the ACAI method (B) and NCAI method (C). A Gaussian kernel was used with a FWHM of 9 voxels. To avoid too much effect of other tissue classes in the NCAI method, we also show the results for NCAI with a Gaussian kernel with a FWHM of 3 voxels (D).

with a limited spatial resolution of PET scanner, image noise, and so on.

Currently, the quality of the MRI segmentation image is always sufficiently high for this application (Van Leemput et al., 1999; D'Agostino et al., 2006; Nelissen et al., 2006). The outcomes of the MRI segmentation are images consisting of the probabilities that a voxel belongs to a tissue class. These probabilities are used by ACAI. Image coregistration is always a key issue in the image processing domain. In our current implementation, the high-resolution anatomical MRI image was coregistered to the low resolution FDG image, but alternatively, the FDG image could be coregistered to the MRI image. The latter approach has the advantage that the segmented GM voxels are unchanged after the coregistration while the former has the advantage that it can be easily combined with the anatomical-based reconstructed PET images (Baete et al., 2004a,b). In our simulation experiment, a perfect coregistration was used since the simulated images were all derived from standard brain phantom. Therefore, our simulation results are not affected by miscoregistration at all. Actually, current registration methods perform very well based on various specialized algorithms such as the mutual information technique (Maes et al., 1999) as is the case in our clinical example. Therefore, we expect that this factor will not lead to large errors in the applications.

The accuracy of determination of homologous regions in the contralateral brain can be easily guaranteed in our simulation experiment, because the brain phantom used for constructing simulated images is a standard template where the mid-plane of the brain is accurately defined. Therefore, the influences of this factor should be negligible in our results. In real images, several different approaches can be used to identify the mid-sagittal plane. One way is to manually define this plane on MRI. Another approach is to use a spatial normalization scheme (e.g. using SPM http://www.fil.ion.ucl.ac.uk/spm/). The latter one is what we adopted in the implementation. By warping the target image to a standard space, the symmetry plane of the brain can be determined automatically.

In some cases, the homologous voxel belongs to a different tissue class. When using a the NCAI method, this is not important as long as we use a kernel width which results in inclusion of voxels mainly belonging to the same tissue class for both homologous voxels. For the ACAI method, this is no problem as long as the kernel contains some voxels of the tissue class of interest. For larger kernels this will always be the case and it is recommended to use sufficient large kernels. In our patient data we used a Gaussian kernel of 9 voxels FWHM.

Some parts in the brain are not symmetrical and the homologous region might be located slightly asymmetrical. This problem can be taken into account by using a parcellation of the brain in volumes of interest (Tzourio-Mazoyer et al., 2002) and to combine it with our ACAI method.

Because of the limited spatial resolution of a PET scanner, the voxel values suffer from the partial volume effect (PVE). Comparing with the homologous region, this might introduce a large asymmetry, which is the case in ROI 2 in our experiment. It is important to note that the ACAI method is not correcting for the partial volume effect, but it can be applied in combination with a partial volume correction technique, e.g. using anatomical-based maximum-a-posteriori reconstruction algorithm (AMAP) (Baete et al., 2004a,b), which can greatly reduce PVE.

Image noise is always inevitable in all medical images. To estimate the influence of image noise, 100 different noise realizations were used in our validation experiment. The standard deviation of the mean AI across 100 images was evaluated at each kernel size in each region of interest. The standard deviation decreases when the area of the ROI increases. In larger ROIs, the standard deviation is relatively small because of the smoothing nature of the convolution and the averaging calculation within each ROI. The worst case is in ROI 1 (size of 0.14 cm^3) where, the standard deviation of AI can be comparable with, or even be larger than the AI of baseline. It means that noise will greatly affect the detection result when the size of the expected region

is small. Care must be taken when interpreting asymmetry data in small regions.

Kernel size

When the kernel size increases, the AI curves of all ROI tend to decrease. Basically there are two reasons: first, larger kernel covers more voxels with normal intensity, which can further reduce the average value in the hyperintense ROI in volumetric images after convolution. Second, image noise can be further minimized by a larger kernel because of its statistical distribution all over the image. A proper kernel size should be comparable to the size of the expected region of interest (Turin, 1960), facilitating the proposed method to obtain relatively large difference between AI of baseline and phantom image, meanwhile keep relatively small residual AI of baseline.

Kernel type

In our study, we only used a Gaussian kernel. However, other types of kernels also can be adopted in ACAI method as long as they have a symmetric structure.

Extension to other tissue classes

In this study, we applied the proposed method using only the gray matter. Its basic idea is easily extended to include other tissue classes and other image modalities beyond FDG-PET. Functional asymmetries from different tissue classes can be calculated at the same time by Eqs. (3–4) and compared as needed. The method can be used for other nuclear medicine brain imaging. The proposed method has great potential to become a useful diagnostic tool in medical imaging.

Conclusion

We proposed a method using prior anatomical information to detect the metabolic asymmetries in FDG-PET images. The advantage of our method is the ability of greatly minimizing the asymmetries caused by anatomical variation, and focusing on the real metabolic abnormalities. Simulation experiment proves the validity of this method and shows its great potential.

References

Aubert-Broche, B., Grova, C., Jannin, P., Buvat, I., Benali, H., Gibaud, B., 2003. Detection of inter-hemispheric asymmetries of brain perfusion in SPECT. Phys. Med. Biol. 48, 1505–1517.

Aubert-Broche, B., Jannin, P., Biraben, A., Bernard, A.-M., Haegelen, C., Prigent Le Jeune, F., Gibaud, F., 2005. Evaluation of methods to detect interhemispheric asymmetry on cerebral perfusion SPECT: application to epilepsy. J. Nucl. Med. 46, 707–713.

Baete, K., Nuyts, J., Van Paesschen, W., Suetens, P., Dupont, P., 2004a. Anatomical based FDG-PET reconstruction for the detection of hypometabolic regions in epilepsy. IEEE Trans. Med. Imag. 23, 510–519.

Baete, K., Nuyts, J., Van Laere, K., Van Paesschen, W., Ceyssens, S., De Ceuninck, L., Gheysens, O., Kelles, A., Van den Eynden, J., Suetens, P., Dupont, P., 2004b. Evaluation of anatomy based reconstruction for partial volume correction in brain FDG-PET. NeuroImage. 23, 305–317.

D'Agostino, E., Maes, F., Vandermeulen, D., Suetens, P., 2006. A unified framework for atlas based brain image segmentation and registration. Lect. Notes Comput. Sci. 4057, 136–143 (Proceedings third international workshop on biomedical image registration — WBIR 2006, July 9–11, 2006, Utrecht, The Netherlands).

Hudson, H., Larkin, R., 1994. Accelerated image reconstruction using ordered subsets of projection data. IEEE Trans. Med. Imag. 13 (4), 601–609.

Kang, K., Lee, D., Cho, J., Lee, J., Yeo, J., Lee, S., Chung, J., Lee, M., 2001. Quantification of F-18 FDG PET images in temporal lobe epilepsy patients using probabilistic brain atlas. NeuroImage 14, 1–6.

Maes, F., Vandermeulen, D., Suetens, P., 1999. Comparative evaluation of multiresolution optimization strategies for multimodality image registration by maximization of mutual information. Med. Image Anal. 3 (4), 373–386.

Nelissen, N., Van Paesschen, W., Baete, K., Van Laere, K., Palmini, A., Van Billoen, H., Dupont, P., 2006. Correlations of interictal FDG-PET metabolism and ictal SPECT perfusion changes in human temporal lobe epilepsy with hippocampal sclerosis. NeuroImage 32, 684–695.

Signorini, M., Paulesu, E., Friston, K., Perani, D., Colleluori, A., Lucignani, G., Grassi, F., Bettinardi, V., Frackowiak, R., Fazio, F., 1999. Rapid assessment of regional cerebral metabolic abnormalities in single subjects with quantitative and nonquantitative [18F]FDG PET: a clinical validation of statistical parametric mapping. NeuroImage 9, 63–80.

Turin, G., 1960. An introduction to matched filters. IRE Trans. Inf. Theory 6, 311–329.

Tzourio-Mazoyer, N., Landeau, B., Papathanassiou, D., Crivello, F., Etard, O., Delcroix, N., Mazoyer, B., Joliot, M., 2002. Automated anatomical labeling of activations in SPM using a macroscopic anatomical parcellation of the MNI MRI single-subject brain. Neuroimage 15, 273–289.

Van Bogaert, P., Massager, N., Tugendhaft, P., Wikler, D., Damhaut, P., Levivier, M., Brotchi, J., Goldman, S., 2000. Statistical parametric mapping of regional glucose metabolism in mesial temporal lobe epilepsy. NeuroImage 12, 129–138.

Van Leemput, K., Maes, F., Vandermeulen, D., Suetens, P., 1999. Automated model based tissue classification of MR images of the brain. IEEE Trans. Med. Imaging 18 (10), 897–908.

Volkau, I., Prakash, B., Ananthasubramaniam, A., Gupta, V., Aziz, A., Nowinski, W., 2006. Quantitative analysis of brain asymmetry by using the divergence measure: normal-pathological brain discrimination. Acad. Radiol. 13, 752–758.